












Propylene glycol inactivates respiratory viruses and prevents airborne transmission

Christine T Styles¹ , Jie Zhou¹, Katie E Flight^{1,†}, Jonathan C Brown¹ , Charlotte Lewis², Xinyu Wang³, Michael Vanden Oever^{1,‡} , Thomas P Peacock¹ , Ziyin Wang¹ , Rosie Millns¹, John S O'Neill⁴ , Alexander Borodavka³ , Joe Grove² , Wendy S Barclay¹, John S Tregoning¹ & Rachel S Edgar^{1,*} 

Abstract

Viruses are vulnerable as they transmit between hosts, and we aimed to exploit this critical window. We found that the ubiquitous, safe, inexpensive and biodegradable small molecule propylene glycol (PG) has robust virucidal activity. Propylene glycol rapidly inactivates a broad range of viruses including influenza A, SARS-CoV-2 and rotavirus and reduces disease burden in mice when administered intranasally at concentrations commonly found in nasal sprays. Most critically, vaporised PG efficiently abolishes influenza A virus and SARS-CoV-2 infectivity within airborne droplets, potently preventing infection at levels well below those tolerated by mammals. We present PG vapour as a first-in-class non-toxic airborne virucide that can prevent transmission of existing and emergent viral pathogens, with clear and immediate implications for public health.

Keywords airborne transmission; influenza; propylene glycol; SARS-CoV-2; virucide

Subject Categories Evolution & Ecology; Microbiology, Virology & Host Pathogen Interaction

DOI 10.15252/emmm.202317932 | Received 28 April 2023 | Revised 16 October 2023 | Accepted 17 October 2023 | Published online 16 November 2023

EMBO Mol Med (2023) 15: e17932

See also: [I Glas & SC David](#) (December 2023)

Introduction

The COVID-19 pandemic has claimed > 6.6 million lives so far (World Health Organization, 2022a), and the World Health Organization estimates seasonal influenza mortality at 290,000–650,000 people annually (World Health Organization, 2022b). Beyond this health burden, respiratory viruses cause severe economic and societal costs, recently estimated for the UK government alone at £23 billion/year during future influenza-type pandemics and £8 billion/year for seasonal

influenza (National Engineering Policy Centre, 2022). Public health and social measures used to combat respiratory virus transmission include mask-wearing, physical distancing, lockdown and travel restrictions (Talic *et al*, 2021). Such measures are primarily evidenced by observational studies rather than randomised controlled trials (Glasziou *et al*, 2021; Hirt *et al*, 2022) and require compliance (Fischer *et al*, 2021; Howard *et al*, 2021). Other strategies involve improving ventilation and frequent disinfection to remove infectious virus from the environment, but both come with significant drawbacks, and there is growing concern over the health and environmental consequences of prolonged, widespread use of disinfectants (Curran *et al*, 2019; Rai *et al*, 2020; BurrIDGE *et al*, 2021; Ghafoor *et al*, 2021; Xiao *et al*, 2022). Natural ventilation is not always suitable, increasing risk from air pollutants and vector-borne diseases along with thermal and energy considerations in colder climates. Expensive engineering solutions like mechanical ventilation require coordinated action across government, health, transport, business, housing and environmental sectors, and a significant culture shift to prioritise infection resilience in indoor environments alongside net zero objectives (National Engineering Policy Centre, 2022). There is an urgent unmet need for novel non-pharmaceutical interventions to combat emerging and seasonal diseases.

Propylene glycol (PG, propan-1,2-diol) is a synthetic liquid compound, whose amphiphilic properties are utilised in a wide range of products and industries: food and drink, cosmetics and pharmaceuticals, including oral, topical, intravenous and nebulised drug delivery (European Medicines Agency, 2014). PG is considered a “Generally Recognised As Safe” (GRAS) molecule, efficiently metabolised and excreted from mammals and is approved for widespread applications by the US Food and Drug Agency (FDA) and European Medicines Agency (EMA) (European Medicines Agency, 2014; Food and Drug Administration (FDA), 2019). PG is largely used as a vehicle or humectant in these preparations due to its water-absorbing properties; however, it has both anti-bacterial (Robertson *et al*, 1942; Puck *et al*, 1943; Nalawade *et al*, 2015) and anti-fungal activity (Faergemann & Fredriksson, 1980; Singh *et al*, 2018). Studies

1 Department of Infectious Disease, Imperial College London, London, UK

2 MRC-University of Glasgow Centre for Virus Research, Glasgow, UK

3 Department of Biochemistry, University of Cambridge, Cambridge, UK

4 MRC Laboratory of Molecular Biology, Cambridge, UK

*Corresponding author. Tel: +44 2075942762; E-mail: rachel.edgar@imperial.ac.uk

†Present address: University College London, London, UK

‡Present address: Life Edit Therapeutics, Morrisville, NC, USA

conducted in the 1940s show PG vapour reduced the infectivity of aerosolised bacterial pathogens in mouse models, preventing sepsis-induced mortality (Robertson *et al*, 1942; Puck *et al*, 1943; Lester *et al*, 1952). In human trials from the same era, vaporised PG reduced the airborne bacterial burden in army barracks (Mather & McClure, 1945), and the introduction of PG vapour on a children's convalescent ward reduced the incidence of undefined respiratory illnesses between 1941 and 1944 (Harris & Strokes, 1945). One study suggested PG vapour could protect mice against disease when exposed to airborne influenza (Robertson *et al*, 1941) and reduce vaccinia- and influenza-mediated fatality in chick embryos (Dunham & MacNeal, 1943; MacNeal & Dunham, 1944). These findings preceded the advent of molecular virology, so the impact of PG on virus particle infectivity was never directly assessed and remains poorly defined.

We tested the hypothesis that PG is virucidal and could reduce respiratory virus transmission by droplet, aerosol and fomite routes.

Results

PG inactivates influenza A virus and reduces disease severity

To examine whether PG exhibits virucidal activity, we first focused on influenza A virus (IAV), a causative agent of seasonal outbreaks in humans and birds that significantly burdens healthcare systems and the poultry farming industry worldwide (World Health Organization, 2022b), and responsible for the worst pandemics of the previous century (Neumann *et al*, 2009). The prototypical IAV lab strain A/PR8/8/34 (henceforth referred to as IAV) was incubated with different concentrations of PG, and infectivity was determined by titration. PG dramatically reduced IAV infection of cultured cells, with virucidal activity dependent on both PG concentration and incubation time (Figs 1A–C and EV1A–C). These results were mirrored with the 2009 influenza pandemic clinical isolate H1N1 A/England/195/09 (E195; Figs 1D–F and EV1D–F). PG-mediated IAV inactivation was temperature-dependent, with progressively greater virucidal activity evident at 32°C (nasal and skin temperature) and 37°C (body temperature) compared with 20°C (room temperature, RT). PG had potent virucidal activity at physiological temperatures, reducing IAV infectivity by ~10,000-fold within 5 min and to undetectable levels after 30 min.

To determine the translational potential of PG-mediated virucidal activity against IAV, we then investigated combined inhalation of the 2009 pandemic strain influenza H1N1 A/California/7/2009 and PG *in vivo*. 20% PG was the lowest concentration to yield statistically significant reduction in IAV infectivity at nasal temperature (Figs 1B and E, and EV1B and E). Therefore, mice were intranasally inoculated with 20% PG alone, IAV alone or IAV and 20% PG in combination, with disease progression tracked over 5 days (Fig 1G). Mice were inoculated immediately after IAV and PG were combined (< 1 min), with negligible PG-mediated inactivation prior to infection (Fig EV5D). Mice receiving PG alone showed no adverse effects over 5 days, consistent with its long-established biological safety in mammals. Following inhalation of IAV alongside PG, mice showed enhanced survival and reduced clinical signs compared to mice that inhaled IAV alone (Figs 1H and EV2). 3/5 mice within the IAV group showed such poor clinical scores that they were humanely

culled 3 days after infection whereas no mice in the IAV + PG group reached this severity limit, demonstrating the protective nature of PG during infection. Mice also lost significantly less weight when PG was co-administered with IAV than with IAV alone (Fig 1I). Analysis of the remaining mice on day 5 post-infection showed PG inhalation reduced clinical score and bronchioalveolar lavage cell counts (Fig EV2A–C), despite equivalent nasal and airway viral loads at this late time post-infection (Fig EV2D and E). Although further investigations are required to determine whether PG treatment reduces peak inflammatory cell infiltrates and viral loads at earlier times post-infection, we conclude that PG can safely reduce the infectivity of influenza A virus *in vitro* and *in vivo*.

PG has broad-spectrum virucidal activity

We next asked whether PG could inactivate other enveloped viruses, including the virus responsible for the COVID-19 pandemic; severe acute respiratory syndrome coronavirus 2 (SARS-CoV-2). We found that PG inactivated the IC19 strain of SARS-CoV-2 (McKay *et al*, 2020) with even greater efficiency than observed for IAV (Figs 1C and F, and 2A). After 1 min treatment with 50% PG at room temperature, SARS-CoV-2 infectivity decreased by > 10,000-fold, indicating clear virucidal activity that persisted over longer time frames (Figs 2A and EV3A). PG also efficiently reduced the infectivity of the enveloped double-stranded DNA gamma-herpesvirus Epstein Barr (EBV), a lifelong infection carried by most of the human population and associated with numerous cancers (Farrell, 2019). Similar to IAV and SARS-CoV-2, PG showed robust virucidal activity against EBV, with > 1,000-fold reduction in viral titre upon incubation with 50% PG (Figs 2B and EV3B).

To explore the broader context of PG's activity against disease-causing viruses, we employed a pseudovirus system engineered to express viral envelope glycoproteins from diverse human pathogens, including NL63 and 229E seasonal coronaviruses, severe acute respiratory syndrome coronavirus (SARS-CoV), middle eastern respiratory syndrome coronavirus (MERS) and Ebola. Using this platform, we also tested PG against glycoproteins from different SARS-CoV-2 variants of concern such as omicron. Using a bioluminescence-based assay for infectivity (Fig 2C), PG significantly limited the infection capability of every different pseudovirus, rapidly reducing entry into susceptible cells in a dose-dependent manner (Fig 2D; Appendix Fig S1). Although PG consistently reduced infectivity, the concentration required varied between the different pseudovirus-expressed glycoproteins, recapitulating the variation in the specific potency of PG against IAV, SARS-CoV-2 and EBV virus particles. This suggests different PG virucidal thresholds and modes of action against specific viruses, but an overall background of broad-spectrum virucidal activity.

One way that PG could restrict infection is by disrupting the viral phospholipid envelope, as shown for bacterial membranes (Rubiano *et al*, 2020). To assess this, we employed a lentivirus-based pseudovirus assay, in which concentrated SARS-CoV-2 (Wuhan strain) pseudovirus was immobilised onto coverslips and then incubated with PG before staining with anti-capsid and anti-glycoprotein antibodies, followed by fluorescently labelled secondary antibodies (Fig 3A). Signal intensity in the capsid and glycoprotein channels was assessed to determine envelope and glycoprotein integrity, with a higher capsid signal indicative of membrane permeabilisation. A

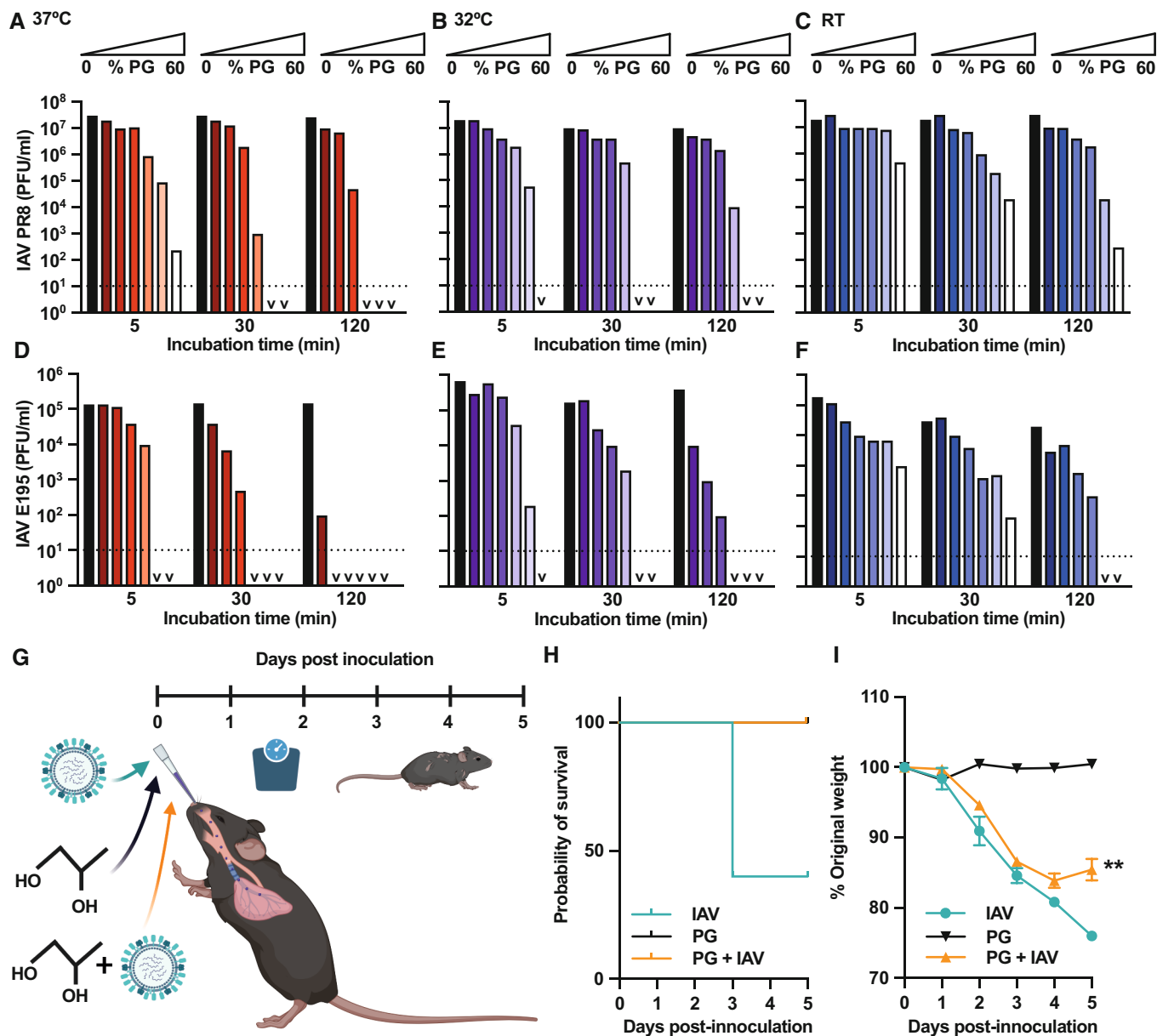


Figure 1. Propylene glycol (PG) reduces influenza A virus infectivity *in vitro* and *in vivo*.

A–F IAV strains PR8 (A–C) and E195 (D–F) were incubated with 0–60% PG for 5–120 min at (A/D) 37°C, (B/E) 32°C or (C/F) room temperature (RT) and infectivity assessed by plaque assay ($N = 2$); PFU = plaque forming units. 2-way ANOVA ([PG] \times time): (A) [PG] **** $P < 0.0001$, time **** $P < 0.0001$, interaction **** $P < 0.0001$; (B) [PG] **** $P < 0.0001$, time **** $P < 0.0001$, interaction *** $P < 0.001$; (C) [PG] **** $P < 0.0001$, time **** $P < 0.0001$, interaction **** $P > 0.0001$. (D) [PG] **** $P < 0.0001$, time **** $P < 0.0001$, interaction *** $P < 0.001$, (E) [PG] **** $P < 0.0001$, time **** $P < 0.0001$, interaction **** $P < 0.0001$. (F) [PG] **** $P < 0.0001$, time **** $P < 0.0001$, interaction **** $P < 0.0001$. $v = < 10^1$; dashed line = limit of detection. Representative replicate shown, see Fig EV1 for repeat.

G *In vivo* methodology. Mice were intranasally inoculated with 50 μ l total volume of 20% PG in PBS, 5×10^4 PFU H1N1 Cal09 IAV in PBS, or 20% PG + IAV and monitored for 5 days ($N = 5$ mice/group; mean \pm SD).

H Mouse survival after infection.

I Weight loss after infection. Mixed-effect analysis: [Time] **** $P < 0.0001$, [PG] **** $P < 0.0001$; IAV alone versus PG + IAV day 5 ** $P = 0.0056$. For % PG (v/v) conversion to g/l or g/kg see Appendix Table S1.

Source data are available online for this figure.

significant loss of SARS-CoV-2 pseudovirus envelope integrity occurs between 65 and 75% PG treatment, with capsid antibody binding at 75% PG solution equivalent to the NP-40 detergent control (Fig 3B and C). The same pattern was observed for pseudovirus

containing glycoprotein from vesicular stomatitis virus (VSV-G; Fig EV4A).

SARS-CoV-2 Wuhan strain pseudovirus infectivity is restricted at PG concentrations above 20% (v/v) and abolished with 40% PG

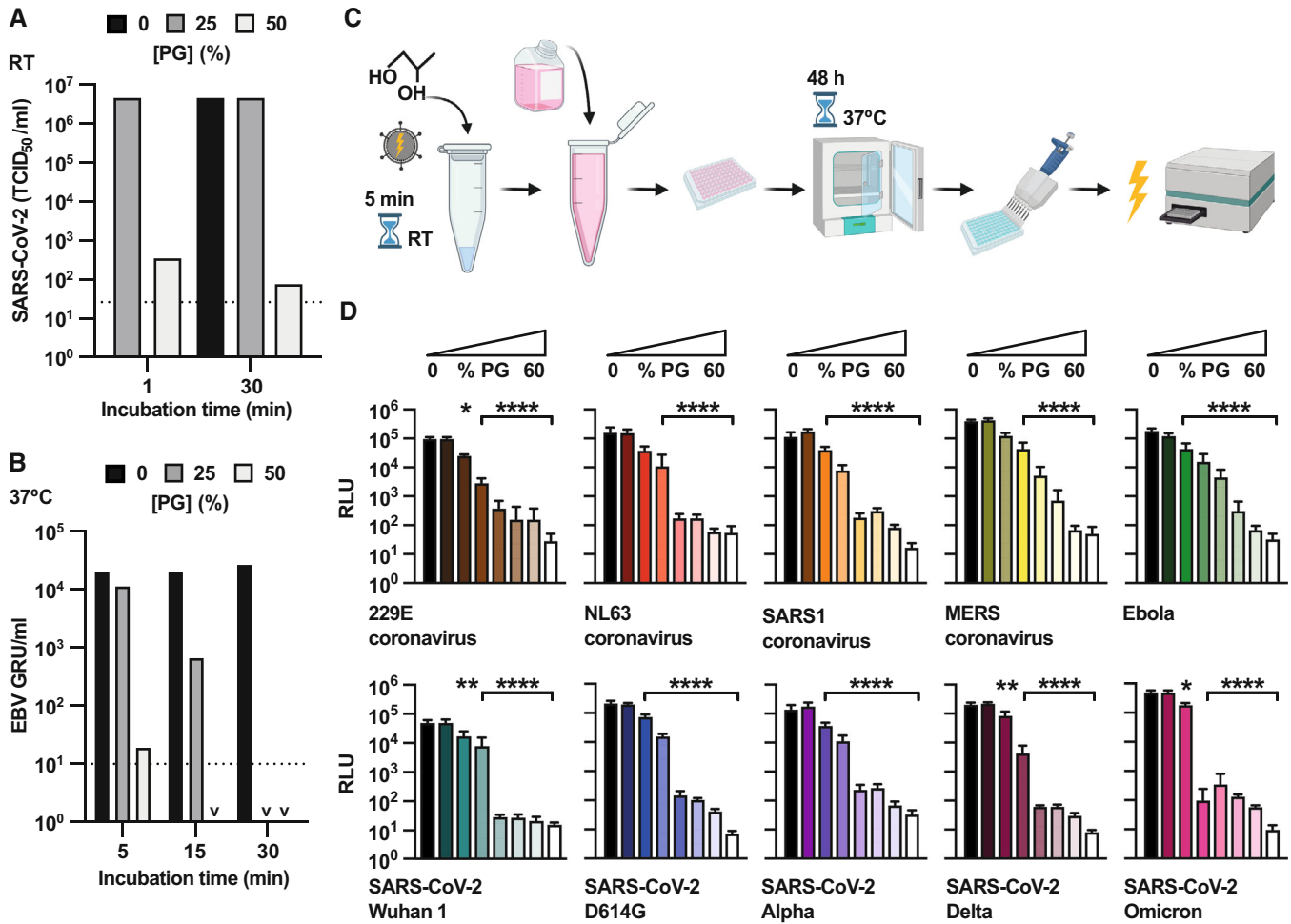


Figure 2. PG inactivates SARS-CoV-2, EBV and many different pseudoviruses.

A SARS-CoV-2 incubated with 0–50% [PG] for 1–30 min at RT and infectivity assessed by TCID₅₀ assay ($N = 2$). 2-way ANOVA ([PG] × time): [PG] **** $P < 0.0001$, time * $P < 0.05$, interaction ** $P < 0.01$. Dotted line = limit of detection. Representative replicate shown, see Fig EV3 for repeat.

B EBV incubated with 0–50% [PG] for 5–30 min at 37°C and infectivity assessed by titration ($N = 2$; GRU = green Raji units). 2-way ANOVA ([PG] × time): [PG] **** $P < 0.0001$, time **** $P < 0.0001$, interaction **** $P < 0.0001$; $v < 10^1$. Representative replicate shown, see Fig EV3 for repeat.

C, D Methodology (C) and results (D) of lentivirus pseudotypes expressing different glycoproteins incubated with 0–60% PG for 5 min at RT before assessing infectivity by bioluminescence ($N = 2$, $n = 3$; mean ± SD). White bars = mock-infected. 1-way ANOVA [PG]: Multiple comparisons ** $P < 0.01$, *** $P < 0.001$, **** $P < 0.0001$.

Source data are available online for this figure.

(Fig 2D), much lower than the PG concentrations required for significant permeabilisation of the viral envelope. Whilst PG-mediated membrane disruption likely contributes to pseudovirus inactivation, direct effects on viral proteins cannot be discounted, although we observed no consistent difference in glycoprotein signal upon PG treatment with the antibodies used in this study (Figs 3B and C, and EV4A). Therefore, we assessed whether PG treatment could reduce the infectivity of non-enveloped rotavirus (RV), a causative agent of severe gastroenteritis in children (Crawford *et al*, 2017). PG could exert a virucidal effect against non-enveloped viruses by altering the structure of surface proteins that mediate host membrane penetration or by direct capsid disruption (Kumar *et al*, 2018). Incubation of the simian RV strain SA11 with PG resulted in time-, temperature- and concentration-dependent virus inactivation (Figs 3D and EV4B), with similar kinetics to enveloped IAV and

EBV (Figs 1A–F, 2B, EV1 and EV3B). This indicates that PG can interfere with viral protein structure to render RV and potentially other non-enveloped viruses non-infectious.

Vaporised PG inactivates airborne viruses

Respiratory droplets and aerosols that are exhaled/expelled by talking, sneezing or coughing from infected individuals represent a major transmission route for many pathogens, particularly respiratory viruses such as influenza and SARS-CoV-2 (Leung, 2021). Artificially generated aerosols of SARS-CoV-2 and IAV remain infectious for at least 3 h and 1 h, respectively (Kormuth *et al*, 2018; van Doremalen *et al*, 2020), with viable SARS-CoV-2 aerosols identified at > 2 m distance from infectious patients (Lednicky *et al*, 2020). The COVID-19 pandemic has highlighted the

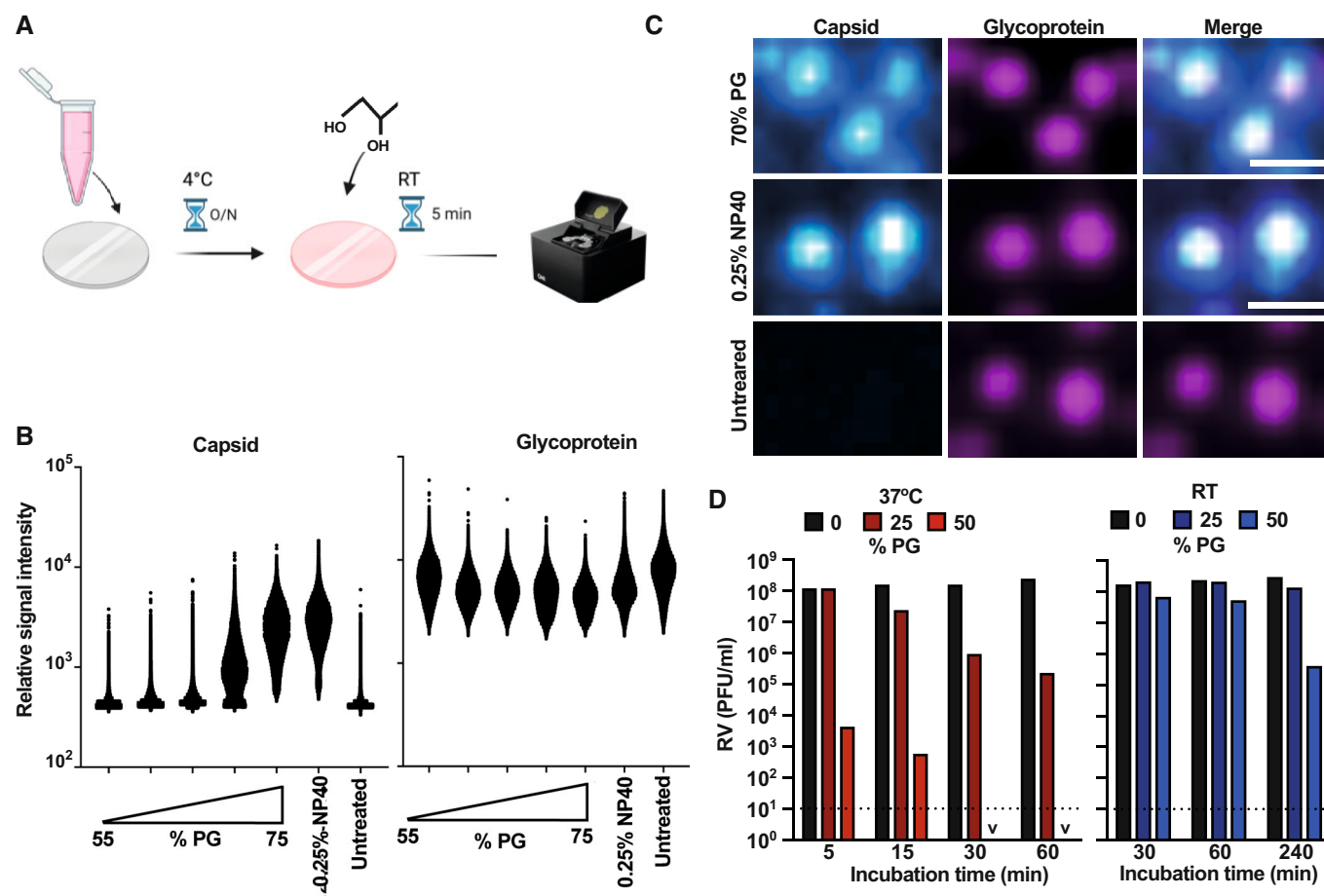


Figure 3. PG mediates viral envelope permeabilisation and inactivates non-enveloped rotavirus (RV).

A, B Methodology (A) and virus particle signal intensities (B) of concentrated SARS-CoV-2 pseudovirus immobilised onto coverslips then incubated with 55–75% [PG] for 5 min at RT ($N = 3$). Pseudovirus particles were stained with anti-capsid and anti-glycoprotein primary antibodies followed by fluorescently labelled secondary antibodies and then imaged using the Oxford Nanoimager at 100 \times oil immersion at 488 and 640 nm.

C Representative enlarged image of immobilised SARS-CoV-2 pseudovirus incubated with 70% PG at RT for 5 min, 0.25% NP40 Cell Lysis Buffer at RT for 5 min or PBS control. “Merge” denotes an overlay of both channels. Scale bar = 400 nm.

D Rotavirus was incubated with 0–50% [PG] for 1–240 min at RT or 37°C and infectivity assessed by titration ($N = 2$); PFU = plaque forming units. 2 way ANOVA ([PG] \times time), 37°C: [PG] **** $P < 0.0001$, time **** $P < 0.0001$, interaction **** $P < 0.0001$, RT: [PG] *** $P < 0.001$, time **** $P < 0.0001$, interaction **** $P < 0.0001$. $v = < 10^1$; dashed line = limit of detection. Representative replicate shown, see Fig EV4 for repeat.

Source data are available online for this figure.

clear and pressing need for effective, safe and economical ways to inactivate infectious particles from contaminated air. Current virucidal disinfectants are unsafe for human consumption and often environmentally harmful (Curran *et al*, 2019; Rai *et al*, 2020; Burrige *et al*, 2021; Ghafoor *et al*, 2021; Xiao *et al*, 2022). PG is biodegradable and non-toxic, with numerous studies showing PG vapour can be safely inhaled for long durations without adverse effects, testing up to 41 mg PG/l air (Robertson & Loosli, 1947; Montharu *et al*, 2010; Werley *et al*, 2011; Fowles *et al*, 2013; Phillips *et al*, 2017; Dalton *et al*, 2018; Langston *et al*, 2021).

The condensation of vapourised or aerosolised PG with airborne aqueous respiratory droplets is very energetically favourable and occurs rapidly in atmospheric air at room temperature. We predicted that low levels of vapourised PG would condense with respiratory droplets in sufficient amounts to inactivate any airborne

virus particles therein. To model infection by airborne IAV and SARS-CoV-2, we used a bespoke transmission tunnel system (Fig 4A) (Singanayagam *et al*, 2020). Within the transmission tunnel, permissive cell monolayers at different distances were exposed to airborne virus droplets (4–6 μ m) in the presence of total vaporised PG concentrations from 0 to 11 mg/l air (Appendix Fig S2). Following exposure, viral plaque area was computationally derived via two independent methods. In line with our predictions and the 1941 pathogenesis study (Robertson *et al*, 1941), PG vapour reduced airborne IAV and SARS-CoV-2 infectivity in a dose-dependent manner (Fig 4B–F, Appendix Fig S3), abolishing infection within a distance of < 1 m. Vapour was a more efficacious virucide than PG in solution (Figs 1A–F, 2, EV1 and EV3), as was PG within nebulised droplets (Figs 1A–C vs. EV5), mirroring inhalation in mice (Fig 1G–I).

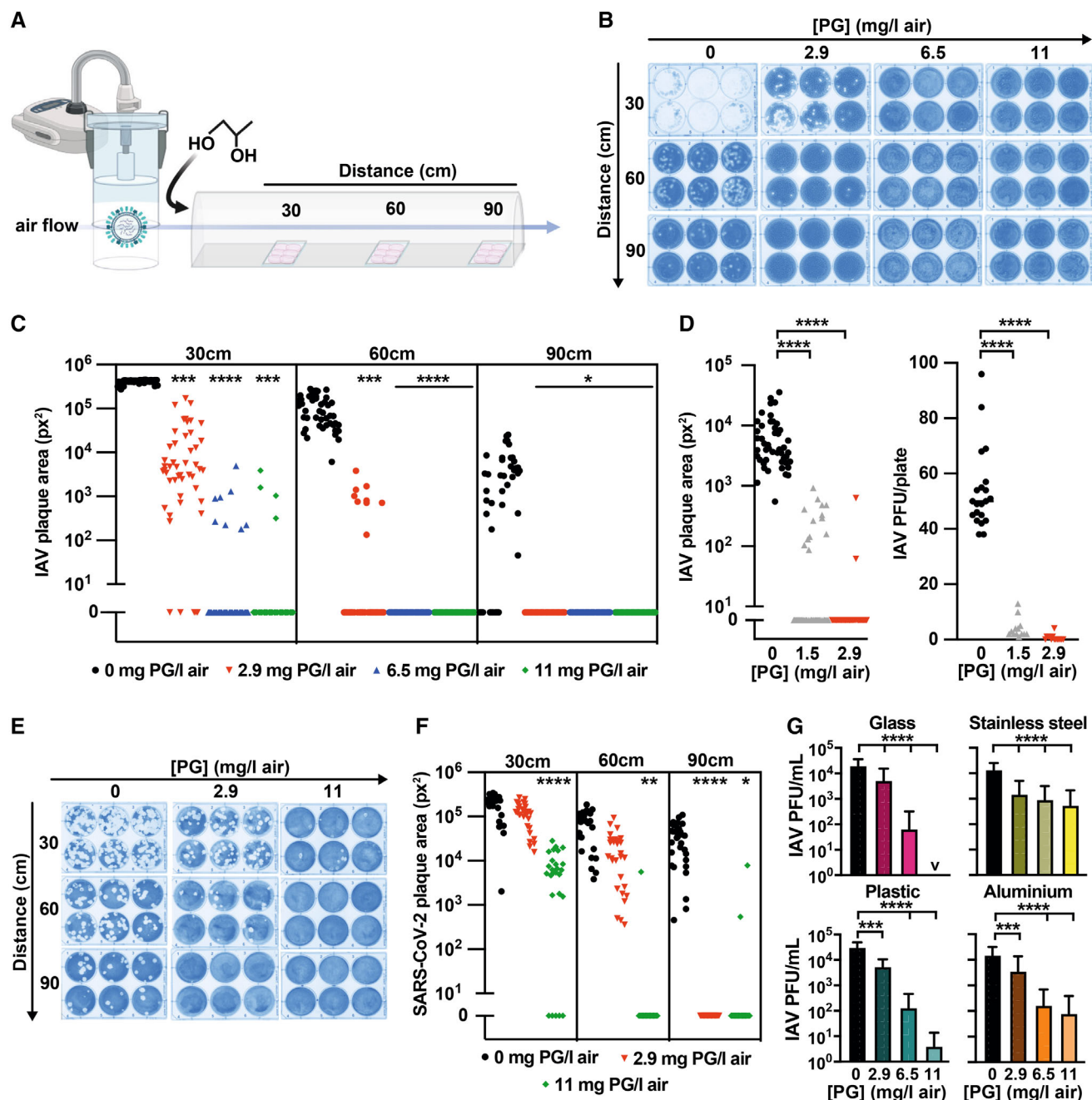


Figure 4. PG vapour efficiently inactivates airborne IAV and SARS-CoV-2.

- A** Virus transmission tunnel schematic.
- B, C** (B) PG vapour was introduced into the transmission tunnel to a final concentration of 0–11 mg/l air prior to nebulisation of 10^6 PFU IAV. Representative IAV culture plates; (C) viral plaque area on culture plates at 30 cm, 60 cm and 90 cm distance was computationally analysed using ImageJ ColonyArea plugin ($N = 8$, $n = 6$); 2-way ANOVA ([PG] × distance): [PG] *****P* < 0.0001, distance *****P* < 0.0001, interaction *****P* < 0.0001.
- D** PG vapour was introduced into the transmission tunnel to a final PG concentration of 0–2.9 mg/l air prior to nebulisation of 10^4 PFU IAV. Viral plaque area at 30 cm distance analysed as for (B) ($N = 8$, $n = 6$); 1-way ANOVA [PG]: *****P* < 0.0001 and plaques counted (1-way ANOVA [PG]: *****P* < 0.0001).
- E, F** (E) PG vapour was introduced into the transmission tunnel to a final concentration of 0–11 mg/l air prior to nebulisation of 3×10^4 PFU SARS-CoV-2 Delta variant. Representative SARS-CoV-2 culture plates; (F) viral plaque area was assessed as per (B) ($N = 5$, $n = 6$); 2-way ANOVA ([PG] × distance): [PG] *****P* < 0.0001, distance *****P* < 0.0001, interaction *****P* < 0.0001.
- G** 10^5 PFU IAV on fomite model surfaces (plastic, stainless steel, aluminium and glass) were exposed to vaporised PG (0–11 mg/l air) and infectivity assessed by plaque assay after 25 min ($N \geq 4$, $n \geq 3$; mean ± SD). 1-way ANOVA [PG]: **P* < 0.05, ***P* < 0.01, ****P* < 0.001, *****P* < 0.0001.

Source data are available online for this figure.

Whilst the transmission tunnel has some limitations as a model of viral dissemination through droplets and aerosols (see Appendix Fig S3), our findings clearly demonstrate efficient and rapid PG-mediated inactivation of airborne IAV and SARS-CoV-2, at virus levels that far exceed the estimated amounts expelled by speaking, coughing or sneezing (Gustin *et al*, 2013; Lindsley *et al*, 2015; Singanayagam *et al*, 2020). 1.5 mg PG/l air was the lowest exposure we could consistently generate with our experimental system, and it effectively abolished infectivity when less IAV was nebulised into the tunnel to mimic an amount comparable to multiple human coughs (Fig 4D; Appendix Fig S3). Given the strong correlation between initial viral dose, infection probability and disease severity (Chu *et al*, 2004; Memoli *et al*, 2015; Watson *et al*, 2015; Han *et al*, 2019; Spinelli *et al*, 2021; Van Damme *et al*, 2021), clinical studies are now required to identify the optimum aerosolised PG levels that effectively reduce viral transmission under “real-world” conditions.

Alongside airborne routes, viruses are also transmitted indirectly via contact with surfaces contaminated by the deposition of virus-containing respiratory droplets and subsequent mechanical transfer to mucous membranes (fomite transmission) (Leung, 2021). Infectious SARS-CoV-2 and SARS-CoV can be recovered up to 72 h after deposition on surfaces, including plastic and stainless steel (van Doremalen *et al*, 2020), and viable H1N1 IAV is recoverable for up to 2 weeks from stainless steel (Thompson & Bennett, 2017). Importantly then, PG vapour inactivated IAV upon varied fomites, with PG at 11 mg/l air sufficient to significantly reduce infectious IAV on all surfaces tested (Fig 4G). As such, we propose PG as the first-in-class example of a safe, inexpensive, and environmentally neutral broad-spectrum virucide, for inactivation of airborne and surface-bound viruses.

Discussion

With the increasing threat from emerging pathogens, we need new tools that can immediately be deployed to attenuate viral transmission within social, healthcare and transport settings. For example, sanitising ambulances between patients caused delays and disruption during the COVID-19 pandemic. PG vapour is a potentially valuable resource for limiting diverse virus infections by multiple routes, including aerosol, droplet and fomite transmission; an economical and effective virucide that is much safer to ingest and inhale compared to other disinfectants and fumigation systems, whilst also avoiding their negative environmental consequences and toxicity (Ghafoor *et al*, 2021). Prospective application of PG as an infection prevention measure requires further investigation beyond laboratory settings, but our results strongly suggest we should leverage its virucidal capacity. PG is already an excipient in non-prescription nasal sprays so this intervention could be rapidly implemented, and vapour generation utilises existing technologies.

This study demonstrates that PG has broad-spectrum virucidal activity, against both enveloped and non-enveloped viruses. Conversely, most conventional antiseptics and disinfectants used within hospitals such as ethanol hand gels exhibit poor activity against non-enveloped viruses including human norovirus and RVs (World Health Organization, 2009). Although beyond the scope of this study, it is of commercial and pharmaceutical interest to determine whether PG mediates virucidal activity against other non-enveloped

viruses and to further refine its mechanistic action against viral envelopes, glycoproteins and/or capsids. Recently, PG was shown to disrupt rotavirus replication factories inside cells, demonstrating the potential sensitivity of phase-separated viroplasm to this small molecule, further extending its potential as a broad-spectrum antiviral with a range of mechanistic approaches (Geiger *et al*, 2021). In addition to virucidal activity, studies from the 1940s suggest PG vapour is bactericidal against many aerosolised bacterial species (Robertson *et al*, 1942; Puck *et al*, 1943; Lester *et al*, 1952). Re-evaluating these findings using modern experimental methodologies is paramount, given the threat from antimicrobial resistance. As PG appears to act via biophysical disruption of lipid membranes or protein structure, this presents a substantial, if not insurmountable, barrier to evolutionary escape by pathogens.

Conclusion

Propylene glycol is already approved for use within pharmaceutical, cosmetic and food industries, yet its inherent virucidal activity has not been examined or exploited. PG in nasal sprays, nebulisers and sanitisers could protect vulnerable individuals, whereas direct inactivation of airborne human viruses by PG vapour could potentially reduce the overall infectious burden and transmission rates in clinical and commercial settings.

Materials and Methods

Cell culture

All media and supplements were supplied by Gibco-Life Technologies, and cells were maintained in a humidified incubator at 37°C with 5% CO₂. Madin-Darby Canine Kidney (MDCK; RRID:CVCL_0422), African green monkey kidney (Vero E6; RRID:CVCL_DX71), human hepatoma-derived 7 cell line (Huh7; RRID:CVCL_B7T1) and human embryonic kidney cells (293T; RRID:CVCL_0063) transduced with an ACE2 lentiviral vector (ACE2-293T, as described previously; Peacock *et al*, 2021b) were routinely cultured in Dulbecco's modified Eagle's Medium (DMEM). Raji cells (human, RRID:CVCL_0511) were cultured in RPMI-1640 medium (RPMI). Media was supplemented with 10% foetal calf serum (FCS), GlutaMAX and penicillin/streptomycin. ACE2-293T cells were additionally supplemented with 1 µg/ml puromycin. Vero E6 cells overexpressing ACE2 and TMPRSS2 (VAT cells, as described previously; Rihn *et al*, 2021), were additionally supplemented with non-essential amino acids, 0.2 mg/ml Hygromycin B and 2 mg/ml Geneticin™ (G418 Sulfate). Cells were routinely tested for mycoplasma contamination using Mycoplasma PCR Detection Kit (Cambridge Bioscience).

IAV infectivity plaque assay

Influenza strain A/PR8/8/34 (H1N1) was primarily used in this study and referred to as IAV, and additional influenza strain A/England/195/09 was referred to as E195 and treated in the same way as IAV. IAV was propagated in confluent MDCK cells in the presence of 1 mg/ml TPCK-treated trypsin (Worthington Bioscience) in serum-free medium (SFM) (DMEM, penicillin/streptomycin and GlutaMAX).

IAV was incubated with 0–60% v/v concentration of propylene glycol (PG) (Sigma) for 5–120 min as described, at either room temperature (RT) or at 32 and 37°C. See Appendix Table S1 for conversion % v/v PG solution to g/l. Following PG treatment, the virus/PG suspensions were serially diluted in SFM with the initial 10^{-1} dilution being the detection limit for IAV infectivity in this assay. Confluent MDCK cells were incubated with each serial dilution for 1 h at 37°C, then input virus was removed by aspiration and cells overlaid with SFM containing 0.14% BSA (Sigma), 0.8% Avicel© (FMC BioPolymer) and 1 mg/ml TPCK-treated trypsin. After 72 h, cells were fixed in 8–10% formalin/PBS, stained with 0.1% toluidine blue (Sigma) and viral plaque forming units (PFU) assessed.

IAV fomite infectivity assay with PG vapour

Two microliter droplets containing 10^5 PFU IAV in SFM were pipetted onto stainless steel discs, polystyrene plastic, aluminium foil sections or glass discs within 6 well plates. Plates were placed in a sealed polystyrene chamber and exposed to vaporised PG (0–11 mg/l air) using a MicroFogger 2 (WorkshopScience). After 25 min, virus was recovered in 1 ml SFM, serially diluted and quantified by plaque assay on MDCK as described above.

EBV infectivity assay

Prototypical laboratory strain Epstein–Barr Virus (EBV) containing a GFP cassette was incubated with 0–50% v/v PG for 5–120 min at 37°C. Following treatment, virus/PG suspensions were serially diluted in RPMI with the initial 10^{-1} dilution being the detection limit for EBV infectivity in this assay. 5×10^4 Raji cells were added to each dilution and incubated for 48 h at 37°C. RPMI containing 20 nM TPA and 5 mM sodium butyrate was added and a viral titre determined after 24 h using fluorescent microscopy to identify GFP-expressing cells (Green Raji units; GRU).

Lentivirus pseudotype infectivity assay

Pseudotype lentiviruses were generated in HEK 293T cells as described previously (Peacock *et al*, 2021b). Briefly, 293T cells were co-transfected with plasmids encoding desired envelope glycoprotein, firefly luciferase reporter (pCSGW) and pCAGGS-GAG-POL using Lipofectamine 3000 (Thermo Fisher) and pseudovirus harvested at 48 h and 72 h post-transfection. A control pseudovirus was also constructed without a viral glycoprotein component (“bald” pseudovirus; Appendix Fig S1). Pseudoviruses used in this study contained glycoproteins from five different SARS-CoV-2 variants (Wuhan-1 (McKay *et al*, 2020), D614G (Zhou *et al*, 2022), Alpha (Zhou *et al*, 2022), Delta (preprint: Newman *et al*, 2021) and Omicron (preprint: Newman *et al*, 2021)), middle eastern respiratory syndrome coronavirus (MERS-CoV) (McKay *et al*, 2020), SARS-CoV (McKay *et al*, 2020), NL63 and 229E coronaviruses (McKay *et al*, 2020), Ebola (Long *et al*, 2015), amphotropic murine leukaemia virus (MLV-A) (Long *et al*, 2015) or Indiana vesicular stomatitis virus (VSV-G) (Long *et al*, 2015).

Pseudoviruses were treated with 0–60% v/v [PG] for 5 min at RT and then diluted in growth media. Pseudoviruses were plated in triplicate onto confluent ACE2-293T cells (SARS-CoV-2 variants, SARS-CoV, NL63, Ebola, MLV-A, VZV-G and “bald”) or Huh7 cells

(MERS-CoV and 229E) and incubated for 48 h. Luciferase activity was measured using a Firefly luciferase assay system kit (Promega), on a FLUOstar Omega plate reader (BMG Labtech). Each analysed plate contained triplicate uninfected cells to control for background luminescence.

SARS-CoV-2 TCID50 infectivity assay

The strain of SARS-CoV-2 used for infectivity assays was SARS-CoV-2/England/IC19 and is henceforth referred to as “SARS-CoV-2” (McKay *et al*, 2020). Vero E6 cells in assay diluent (DMEM, 0.3% BSA, NEAA, penicillin/streptomycin) were seeded into 96-well plates and incubated at 37°C for 24 h. SARS-CoV-2 was incubated with 0–50% v/v PG for 1–30 min at RT. Virus/PG suspension was then added to the first column of confluent Vero E6 cells and a \log_{10} /half- \log_{10} dilution series immediately performed in assay diluent. Technical replicates were performed for each sample. Plates were incubated for 5 days before adding an equal volume of crystal violet stain (0.1% w/v) to live cells. Wells were scored for either an intact, stained cell sheet or the absence of cells due to virus-induced cytopathic effect. For each condition, the Spearman-Kärber method was used to calculate the 50% tissue culture infectious dose (TCID50) of virus.

Rotavirus TCID50 infectivity assay

Group A rotavirus (RV, simian strain SA11 G3P[2]) was incubated with 0–50% PG for 1–240 min at RT or 37°C. After PG incubation, RV was serially diluted with serum-free DMEM (supplemented with 0.5 mg/ml porcine trypsin, penicillin/streptomycin, NEAA, and GlutaMAX) and applied to confluent monolayers of green monkey kidney cells (MA104, RRID:CVCL_3846) seeded in 48-well plates. Five days after infection, the number of wells with cells showing virus-induced cytopathic effect (CPE) was recorded. Tissue culture infectious dose 50% (TCID50) was calculated using the Reed and Muench method and converted to plaque-forming units (PFU) by multiplying a conversion factor of 0.70 PFU/TCID50 (Distefano *et al*, 1995).

Pseudovirus membrane permeability assay

HEK293T cells were co-transfected with an HIV packaging construct (pCMV-dR891), a luciferase reporter plasmid (CSLW) and 200 ng/ μ l of an expression vector encoding VSV-G or SARS-CoV-2 Wuhan Spike glycoprotein. Supernatants were collected and filtered at 48/72 h post-transfection and pooled before centrifugation at 86,363 g for 2 h at 4°C using a TH-641 Swinging Bucket Rotor (Thermo Fisher Scientific). The viral pellet was resuspended in 1,000 μ l of OptiMEM (Gibco). 25 mm coverslips were sequentially washed in ddH₂O, ethanol, and methanol for 2 min, then rinsed in acetone and treated with 2% 3-amino-propyltriethoxysilane (diluted in acetone) for 5 min, rinsed twice in ddH₂O, then mounted in Attofluor chambers (Thermo Fisher Scientific). 150 μ l of concentrated virus and 150 μ l of PBS was added to the coverslips then incubated overnight on a shaker at 4°C. They were then rinsed in PBS and fixed in 4% EM-grade formaldehyde (Thermo Scientific, diluted in PBS) for 10 min, then rinsed 3 \times with PBS, treated with PG (diluted in PBS as described) at RT for 5 min and rinsed 10 \times with PBS. Samples were blocked with 2% BSA/PBS (Thermo Scientific) for 10 min, rinsed 3 \times with PBS and incubated

for 1 h with mouse anti-SARS-CoV-2 spike antibody (clone 1A9; Genetex Inc. [GTX632604], 1 µg/ml) or anti-VSV-G glycoprotein antibody (Clone 8G5F11; Kerafast [EB0010], 0.25 µg/ml) diluted in PBS, on a rocker at RT. Following incubation, samples were rinsed twice with PBS, fixed with formaldehyde as described above and permeabilised for 5 min as required using NP40 Cell Lysis Buffer (Invitrogen) diluted 1 in 3 in PBS. Samples were then blocked as described above, rinsed 3× with PBS and incubated for 1 h with anti-HIV1 p55 + p24 + p17 antibody (Abcam [ab63917], diluted 1:4,000 in PBS) on a rocker at RT. Samples were then rinsed 3× with PBS and incubated with Goat anti-Mouse IgG Alexa Fluor 647 (Invitrogen [A32728], 5 µg/ml) and Goat anti-Rabbit IgG Alexa Fluor 488 (Invitrogen [A32731], 5 µg/ml) on a rocker at RT. Samples were rinsed 3× with PBS and post-fixed. Samples were imaged on an Oxford Nanoimager with 100× oil immersion at 488 nm (Alexa Fluor 488) and 640 nm (Alexa Fluor 647) laser illumination. Images were captured from across several regions of the coverslip, with each image covering a 50 µm × 80 µm area. Images were analysed using FIJI (Schindelin *et al*, 2012). Virus particles were identified using the Find Maxima function, using either the GagPol capsid (488 nm) or glycoprotein (640 nm) channels as reference, according to the experiment. Signal intensities were measured in each channel for every particle. Typically, > 10,000 virus particles were quantified per coverslip sample.

Virus transmission tunnel experiments with airborne IAV and SARS-CoV-2

A custom-built transmission tunnel system described by Singanayagam *et al* (2020) (Fig 4A) was used to assess aerosolised PG-mediated inactivation of nebulised IAV and SARS-CoV-2 (B.1.617.2, Delta variant; preprint: Peacock *et al*, 2021a) viruses. Briefly, the transmission tunnel holds 3 tissue culture plates at intervals of 30, 60 and 90 cm from the nebuliser (Aerogen Pro nebuliser; Aerogen). A bias flow pump maintains directional airflow from the nebuliser chamber to the exposure tunnel that deposits airborne virus within 4–6 µm diameter droplets across the tissue culture plates during a 10 min exposure period.

All transmission tunnel experiments were performed within a class I (SARS-CoV-2) or class II (IAV) biological safety cabinet. MDCK or VAT cells were seeded into 6 well plates for IAV or SARS-CoV-2 analysis, respectively. Before placing in the transmission tunnel, MDCK cells were transferred to SFM and VAT cells were transferred to assay medium (MEM, penicillin/streptomycin, 4 mM L-glutamine, 0.4% (w/v) BSA, 0.32% NaHCO₂ and 20 mM HEPES). To assess inactivation of IAV and SARS-CoV-2 by aerosolised PG, concentrations between 0 and 11 mg/l air were introduced into the exposure tunnel using a MicroFogger 2 (WorkshopScience). To quantify the total airborne PG concentration (vapour plus droplets), sampling was performed using a SKC biosampler attached to the tunnel that collected PG into 1 ml distilled water. Samples were analysed on an Osmomat 3000 (Gonotec) and total PG concentration calculated by comparison to a standard curve of PG concentrations (Appendix Fig S2). After PG was aerosolised within the tunnel, permissive cells were exposed to either 10⁴–10⁶ PFU nebulised IAV in PBS or 3 × 10⁴ nebulised PFU SARS-CoV-2 in PBS by starting the directional airflow for 10 min. Cells were then incubated for 1 h at 37°C and 5% CO₂ in a humidified incubator. For IAV, exposed medium was aspirated and cells overlaid with SFM supplemented with 0.8% v/w Avicel© and

before fixation and staining 72 h later as previously described. For SARS-CoV-2, assay medium supplemented with Avicel© (0.75% w/v final concentration) was added directly to cells and incubated for 72 h before cells were fixed and stained with crystal violet (0.1% w/v) containing 30% EtOH for > 30 min.

Transmission tunnel tissue culture plates were imaged using a Bio-Rad Gel Visualiser and each well within the plate was independently computationally analysed. Virus-mediated clearance of cells (plaque area) was quantified using two independent ImageJ FIJI platform systems (Schindelin *et al*, 2012); the plugin ColonyArea (Guzmán *et al*, 2014) and the macro viral plaque (Cacciabue *et al*, 2019). ColonyArea quantifies the % well area containing stained cells and viral plaque quantifies the % area lacking stained cells due to viral cytopathic effect. Calculations were consistently between the two methods (Fig 4 and Appendix Fig S3; Appendix Fig S3D for correlation). Data are presented as plaque area in square pixels (px²). Plaque area shows a strong linear correlation with plaque number at lower viral inputs ($R^2 = 0.72$, Spearman's $r = 0.98$, $P < 0.0001$), that becomes non-linear at higher viral inputs as plaques begin to overlap. To encompass the broadest dynamic range, plaque area is reported for transmission tunnel data.

To assess PG-mediated inactivation of IAV during aerosolisation (Fig EV5), PBS (0% PG control) or 40% PG was added to 10⁶ PFU and then immediately nebulised into the chamber (< 1 min incubation at RT), MDCK cells exposed to the aerosolised PG/IAV mixture and infectious IAV quantified as above.

Combined inhalation of PG and IAV *in vivo*

Six to eight-week-old female BALB/c mice (RRID:IMSR_JAX:000651) were obtained from Charles River UK Ltd (Portsmouth, UK) and kept in specific-pathogen-free (SPF) conditions in accordance with United Kingdom's Home Office guidelines. Mice were maintained in autoclaved individually ventilated cages (IVC) under positive pressure. Mice were housed in groups of five animals per cage with *ad libitum* access to food and water. All work was approved by the Animal Welfare and Ethical Review Board (AWERB) at Imperial College London.

For infections, adult mice were anaesthetised using isoflurane and inoculated intranasally (i.n.) with 50 µl final volume of either 5 × 10⁴ PFU H1N1 A/California/7/2009 influenza virus (IAV), 5 × 10⁴ IAV and 20% PG, or 20% PG alone in sterile PBS (see Appendix Table S1 for conversion of % v/v PG solution to g/kg mouse weight). Mice were inoculated immediately after IAV and PG were mixed. Mice were weighed after infection. Mice were scored for signs of clinical illness after infection based on an adapted scoring system (Graham *et al*, 1991). Scores were given (0–5, with 0 being in healthy condition) for coat, activity, stance and breathing. Investigators were not blinded to treatment. Mice were culled using 100 µl intraperitoneal pentobarbitone (20 mg dose, Pentoject, Animalcare Ltd. UK), and tissues collected and cells in bronchoalveolar lavage (BAL) were counted as previously described (Groves *et al*, 2018). Nasal lavage and BAL were processed for viral load by plaque assay on MDCK cells as described above.

Virus biological safety levels

All experiments with IAV, EBV, RV and pseudoviruses were conducted in class 2 microbiology safety cabinets in Biological

The paper explained

Problem

Viruses pose a tremendous threat to the worldwide population. Interventions that reduce virus transmission such as lockdowns or social distancing are highly disruptive to society and upgrading ventilation systems is costly. Additionally, there are substantial health and environmental concerns with continuous use of current disinfectants.

Results

In this study, we show the widely used, inexpensive and biodegradable non-toxic molecule propylene glycol prevents infection by many different human viruses, including SARS-CoV-2 and influenza A virus. In mouse models where influenza was introduced via the nose, the application of PG along with influenza reduced clinical symptoms of disease and increased survival. Furthermore, safe levels of PG vapour neutralised viruses within airborne and surface droplets.

Impact

Propylene glycol vapour could be used to reduce the amount of airborne virus, therefore limiting transmission of respiratory viruses such as influenza and SARS-CoV-2, the causative agent of the COVID-19 pandemic. Additionally, PG is often included as a “non-active” ingredient in nasal sprays, and this could provide individuals with protection from infection. Although further testing is required outside the laboratory, our data suggest that PG is a valuable weapon in our arsenal to combat the spread of existing and emerging human diseases.

Safety Level 2 laboratories. All experiments with SARS-CoV-2 were conducted in a class 1 microbiology safety cabinet in a Biological Safety Level 3 laboratory.

Statistical analysis

Data were analysed in GraphPad Prism and presented as mean \pm standard deviation (SD) or representative replicate data as noted. At least 2 independent biological replicates were performed for each experimental condition, of which details can be found in respective figure legends and summarised in Appendix Table S2. Statistical tests for virus assays were performed on log₁₀-transformed data ($Y = \log_{10}[Y + 1]$). Detailed information for one-way and two-way ANOVA analyses including F values, degrees of freedom and replicate details is shown in Appendix Table S2. Statistical test outcomes including multiple comparisons are summarised in Appendix Table S3. Investigators were not blinded to treatment during *in vivo* experiments.

Graphics

Synopsis, Figs 1G, 2C, 3A and 4A graphics were created with [BioRender.com](https://www.bio-render.com).

Data availability

This study includes no data deposited in external repositories.

Expanded View for this article is available [online](https://www.embopress.org/doi/10.1002/emmm.202301008).

Acknowledgements

The authors thank R Frise and D Reuss for the discussion, R White and P Farrell for Raji cells and P McKay for codon-optimised spike proteins used to generate pseudoviruses. We also thank N Gunawardana, T Santarius, F Harris and their teams at Addenbrooke's Hospital, Cambridge, whose care of RSE enabled this research to continue. The authors also thank their funding bodies. RSE and CTS are supported by a Royal Society-Wellcome Trust Sir Henry Dale Fellowship (208790/Z/17/Z). JSO is supported by the Medical Research Council, part of United Kingdom Research and Innovation (MRC/UKRI) (MC_UP_1201/4). CL is supported by MRC/UKRI Centre for Virus Research (MC_UU_12014). AB is supported by a Royal Society-Wellcome Trust Sir Henry Dale Fellowship (213437/Z/18/Z). JG is supported by a Royal Society-Wellcome Trust Sir Henry Dale Fellowship (107653/Z/15/Z). RM was supported by a Royal Society of Chemistry Studentship. This study was conducted as part of G2P-UK National Virology consortium funded by MRC/UKRI (MR/W005611/1). The influenza virus transmission tunnel was designed and developed with funding from NC3R. The Oxford Nanoimager was funded by an MRC Capital Award.

Author contributions

Christine T Styles: Data curation; formal analysis; supervision; investigation; visualization; methodology; writing – original draft; writing – review and editing. **Jie Zhou:** Investigation; methodology; writing – review and editing. **Katie E Flight:** Investigation; methodology; writing – review and editing. **Jonathan C Brown:** Formal analysis; investigation; methodology; writing – review and editing. **Charlotte Lewis:** Formal analysis; investigation; visualization; methodology; writing – review and editing. **Xinyu Wang:** Formal analysis; investigation; methodology; writing – review and editing. **Michael Vanden Oever:** Investigation; methodology; writing – review and editing. **Thomas P Peacock:** Investigation; methodology; writing – review and editing. **Ziyin Wang:** Investigation; writing – review and editing. **Rosie Millns:** Investigation; writing – review and editing. **John S O'Neill:** Supervision; funding acquisition; project administration; writing – review and editing. **Alexander Borodavka:** Supervision; funding acquisition; methodology; project administration; writing – review and editing. **Joe Grove:** Supervision; funding acquisition; methodology; project administration; writing – review and editing. **Wendy S Barclay:** Supervision; funding acquisition; methodology; project administration; writing – review and editing. **John S Tregoning:** Formal analysis; supervision; methodology; project administration; writing – review and editing. **Rachel S Edgar:** Conceptualization; data curation; formal analysis; supervision; funding acquisition; visualization; methodology; writing – original draft; project administration; writing – review and editing.

Disclosure and competing interests statement

The authors declare that they have no conflict of interest.

For more information

<https://www.imperial.ac.uk/people/rachel.edgar>.

References

- Burridge HC, Bhagat RK, Stettler MEJ, Kumar P, De Mel I, Demis P, Hart A, Johnson-Llambias Y, King MF, Klymenko O *et al* (2021) The ventilation of buildings and other mitigating measures for COVID-19: a focus on wintertime. *Proc Math Phys Eng Sci* 477: 20200855
- Cacciabue M, Currá A, Gismondi MI (2019) ViralPlaQue: a Fiji macro for automated assessment of viral plaque statistics. *PeerJ* 7: e7729

- Chu CM, Poon LLM, Cheng VCC, Chan KS, Hung IFN, Wong MML, Chan KH, Leung WS, Tang BSF, Chan VL et al (2004) Initial viral load and the outcomes of SARS. *CMAJ* 171: 1349–1352
- Crawford SE, Ramani S, Tate JE, Parashar UD, Svensson L, Hagbom M, Franco MA, Greenberg HB, O’Ryan M, Kang G et al (2017) Rotavirus infection. *Nat Rev Dis Primers* 3: 17083
- Curran ET, Wilkinson M, Bradley T (2019) Chemical disinfectants: controversies regarding their use in low risk healthcare environments (part 1). *J Infect Prev* 20: 76–82
- Dalton P, Soreth B, Maute C, Novaleski C, Banton M (2018) Lack of respiratory and ocular effects following acute propylene glycol exposure in healthy humans. *Inhal Toxicol* 30: 124–132
- Distefano DJ, Gould SL, Munshi S, Robinson DK (1995) Titration of human-bovine rotavirus reassortants using a tetrazolium-based colorimetric end-point dilution assay. *J Virol Methods* 55: 199–208
- Dunham WB, MacNeal WJ (1943) Inactivation of vaccinia virus by mild antiseptics. *J Lab Clin Med* 28: 947–953
- European Medicines Agency (2014) Background review for the excipient propylene glycol. Vol. 44. European Union
- Faergemann J, Fredriksson T (1980) Antimycotic activity of propane-1,2-diol (propylene glycol). *Med Mycol* 18: 163–166
- Farrell PJ (2019) Epstein–Barr virus and cancer. *Annu Rev Pathol* 14: 29–53
- Fischer CB, Adrien N, Silguero JJ, Hopper JJ, Chowdhury AI, Werler MM (2021) Mask adherence and rate of COVID-19 across the United States. *PLoS One* 16: e0249891
- Food and Drug Administration (FDA) (2019) CFR code of federal regulations title 21. Food and Drugs. Vol. 3. <http://www.fda.gov>
- Fowles JR, Banton MI, Pottenger LH (2013) A toxicological review of the propylene glycols. *Crit Rev Toxicol* 43: 363–390
- Geiger F, Acker J, Papa G, Wang X, Arter WE, Saar KL, Erkamp NA, Qi R, Bravo JP, Strauss S et al (2021) Liquid–liquid phase separation underpins the formation of replication factories in rotaviruses. *EMBO J* 40: e107711
- Ghafoor D, Khan Z, Khan A, Ualiyeva D, Zaman N (2021) Excessive use of disinfectants against COVID-19 posing a potential threat to living beings. *Curr Res Toxicol* 2: 159–168
- Glasziou PP, Michie S, Fretheim A (2021) Public health measures for covid-19. *BMJ* 375: n2729
- Graham BS, Bunton LA, Wright PF, Karzon DT (1991) Role of T lymphocyte subsets in the pathogenesis of primary infection and rechallenge with respiratory syncytial virus in mice. *J Clin Invest* 88: 1026–1033
- Groves HT, McDonald JU, Langat P, Kinnear E, Kellam P, McCauley J, Ellis J, Thompson C, Elderfield R, Parker L et al (2018) Mouse models of influenza infection with circulating strains to test seasonal vaccine efficacy. *Front Immunol* 9: 126
- Gustin KM, Katz JM, Tumpey TM, Maines TR (2013) Comparison of the levels of infectious virus in respirable aerosols exhaled by ferrets infected with influenza viruses exhibiting diverse transmissibility phenotypes. *J Virol* 87: 7864–7873
- Guzmán C, Bagga M, Kaur A, Westermarck J, Abankwa D (2014) ColonyArea: an ImageJ plugin to automatically quantify colony formation in clonogenic assays. *PLoS One* 9: e92444
- Han A, Czajkowski LM, Donaldson A, Baus HA, Reed SM, Athota RS, Bristol T, Rosas LA, Cervantes-Medina A, Taubenberger JK et al (2019) A dose-finding study of a wild-type influenza A(H3N2) virus in a healthy volunteer human challenge model. *Clin Infect Dis* 69: 2082–2090
- Harris TN, Strokes J (1945) Summary of a 3-year study of the clinical applications of the disinfection of air by glycol vapors. *Am J Med Sci* 209: 152–155
- Hirt J, Janiaud P, Hemkens LG (2022) Randomized trials on non-pharmaceutical interventions for COVID-19: a scoping review. *BMJ Evid Based Med* 27: 334–344
- Howard J, Huang A, Li Z, Tufekci Z, Zdimar V, van der Westhuizen HM, von Delft A, Price A, Fridman L, Tang LH et al (2021) An evidence review of face masks against COVID-19. *Proc Natl Acad Sci USA* 118: e2014564118
- Kormuth KA, Lin K, Prussin AJ, Vejerano EP, Tiwari AJ, Cox SS, Myerburg MM, Lakdawala SS, Marr LC (2018) Influenza virus infectivity is retained in aerosols and droplets independent of relative humidity. *J Infect Dis* 218: 739–747
- Kumar CS, Dey D, Ghosh S, Banerjee M (2018) Breach: host membrane penetration and entry by nonenveloped viruses. *Trends Microbiol* 26: 525–537
- Langston T, Randazzo J, Kogel U, Hoeng J, Martin F, Titz B, Guedj E, Schneider T, Prabhakar B, Zhang J et al (2021) Thirteen-week nose-only inhalation exposures of propylene glycol aerosols in Sprague Dawley rats with a lung systems toxicology analysis. *Toxicol Res Appl* 5: 239784732110210
- Lednický JA, Lauzard M, Fan ZH, Jutla A, Tilly TB, Gangwar M, Usmani M, Shankar SN, Mohamed K, Eiguren-Fernandez A et al (2020) Viable SARS-CoV-2 in the air of a hospital room with COVID-19 patients. *Int J Infect Dis* 100: 476–482
- Lester W, Dunklin E, Robertson OH (1952) Bactericidal effects of propylene and triethylene glycol vapors on airborne *Escherichia coli*. *Science* 115: 382
- Leung NHL (2021) Transmissibility and transmission of respiratory viruses. *Nat Rev Microbiol* 19: 528–545
- Lindsley WG, Noti JD, Blachere FM, Thewlis RE, Martin SB, Othumpangat S, Noorbakhsh B, Goldsmith WT, Vishnu A, Palmer JE et al (2015) Viable influenza A virus in airborne particles from human coughs. *J Occup Environ Hyg* 12: 107–113
- Long J, Wright E, Molesti E, Temperton N, Barclay W (2015) Antiviral therapies against Ebola and other emerging viral diseases using existing medicines that block virus entry. *F1000Res* 4: 30
- MacNeal WJ, Dunham WB (1944) Inactivation of influenza virus by mild antiseptics. *J Immunol* 49: 123–128
- Mather JM, McClure AD (1945) Experiences with the use of propylene glycol as a bactericidal aerosol in an R.C.A.F. Barracks. *Can J Public Health* 36: 181–187
- McKay PF, Hu K, Blakney AK, Samnuan K, Brown JC, Penn R, Zhou J, Bouton CR, Rogers P, Polra K et al (2020) Self-amplifying RNA SARS-CoV-2 lipid nanoparticle vaccine candidate induces high neutralizing antibody titers in mice. *Nat Commun* 11: 3523
- Memoli MJ, Czajkowski L, Reed S, Athota R, Bristol T, Proudfoot K, Fargis S, Stein M, Dunfee RL, Shaw PA et al (2015) Validation of the wild-type influenza A human challenge model H1N1pdmMIST: An A(H1N1) pdm09 dose-finding investigational new drug study. *Clin Infect Dis* 60: 693–702
- Montharu J, Le Guellec S, Kittel B, Rabemampianina Y, Guillemain J, Gauthier F, Diot P, De Monte M (2010) Evaluation of lung tolerance of ethanol, propylene glycol, and sorbitan monooleate as solvents in medical aerosols. *J Aerosol Med Pulm Drug Deliv* 23: 41–46
- Nalawade T, Sogi SH, Bhat K (2015) Bactericidal activity of propylene glycol, glycerine, polyethylene glycol 400, and polyethylene glycol 1000 against selected microorganisms. *J Int Soc Prev Community Dent* 5: 114–119
- National Engineering Policy Centre (2022) Infection resilient environments: time for a major upgrade
- Neumann G, Noda T, Kawaoka Y (2009) Emergence and pandemic potential of swine-origin H1N1 influenza virus. *Nature* 459: 931–939
- Newman J, Thakur N, Peacock TP, Bialy D, Elrefaey AM, Bogaardt C, Horton DL, Ho S, Kankeyan T, Carr C et al (2021) Neutralising antibody activity

- against SARS-CoV-2 variants, including Omicron, in an elderly cohort vaccinated with BNT162b2. *medRxiv* <https://doi.org/10.1101/2021.12.23.21268293> [PREPRINT]
- Peacock TP, Brown JC, Zhou J, Thakur N, Newman J, Kugathasan R, Sukhova K, Kaforou M, Bailey D, Barclay WS (2021a) The SARS-CoV-2 variant, Omicron, shows rapid replication in human primary nasal epithelial cultures and efficiently uses the endosomal route of entry. *bioRxiv* <https://doi.org/10.1101/2021.12.31.474653> [PREPRINT]
- Peacock TP, Goldhill DH, Zhou J, Baillon L, Frise R, Swann OC, Kugathasan R, Penn R, Brown JC, Sanchez-David RY et al (2021b) The furin cleavage site in the SARS-CoV-2 spike protein is required for transmission in ferrets. *Nat Microbiol* 6: 899–909
- Phillips B, Titz B, Kogel U, Sharma D, Leroy P, Xiang Y, Vuillaume G, Lebrun S, Sciuscio D, Ho J et al (2017) Toxicity of the main electronic cigarette components, propylene glycol, glycerin, and nicotine, in Sprague–Dawley rats in a 90-day OECD inhalation study complemented by molecular endpoints. *Food Chem Toxicol* 109: 315–332
- Puck TT, Robertson OH, Lemon HM (1943) The bactericidal action of propylene glycol vapor on microorganisms suspended in air: II. The influence of various factors on the activity of the vapor. *J Exp Med* 78: 387–406
- Rai NK, Ashok A, Akondi BR (2020) Consequences of chemical impact of disinfectants: safe preventive measures against COVID-19. *Crit Rev Toxicol* 50: 513–520
- Rihn SJ, Merits A, Bakshi S, Turnbull ML, Wickenhagen A, Alexander AJT, Baillie C, Brennan B, Brown F, Bruncker K et al (2021) A plasmid DNA-launched SARS-CoV-2 reverse genetics system and coronavirus toolkit for COVID-19 research. *PLoS Biol* 19: e3001091
- Robertson OH, Loosli CG (1947) Tests for the chronic toxicity of propylene glycol and triethylene glycol on monkeys and rats by vapor inhalation and oral administration. *J Pharmacol Exp Ther* 91: 52–76
- Robertson OH, Loosli CG, Puck TT, Bigg E, Miller BF (1941) The protection of mice against infection with air-borne influenza virus by means of propylene glycol vapor. *Science* 1979: 94
- Robertson OH, Bigg E, Puck TT, Miller BF (1942) The bactericidal action of propylene glycol vapor on microorganisms suspended in air. *J Exp Med* 75: 593–610
- Rubiano ME, Maillard JY, Rubino JR, Ijaz MK (2020) Use of a small-scale, portable test chamber for determining the bactericidal efficacy of aerosolized glycol formulations. *Lett Appl Microbiol* 70: 356–364
- Schindelin J, Arganda-Carreras I, Frise E, Kaynig V, Longair M, Pietzsch T, Preibisch S, Rueden C, Saalfeld S, Schmid B et al (2012) Fiji: an open-source platform for biological-image analysis. *Nat Methods* 9: 676–682
- Singanayagam A, Zhou J, Elderfield RA, Frise R, Ashcroft J, Galiano M, Miah S, Nicolaou L, Barclay WS (2020) Characterising viable virus from air exhaled by H1N1 influenza-infected ferrets reveals the importance of haemagglutinin stability for airborne infectivity. *PLoS Pathog* 16: 1–21
- Singh AD, Debnath C, Banerjee A, Batabyal K, Roy B, Samanta I (2018) Effects of propylene glycol and magnesium chloride against dermatophytes isolated from companion animals. *Indian J Anim Health* 57: 213
- Spinelli MA, Glidden DV, Gennatas ED, Bielecki M, Beyrer C, Rutherford G, Chambers H, Goosby E, Gandhi M (2021) Importance of non-pharmaceutical interventions in lowering the viral inoculum to reduce susceptibility to infection by SARS-CoV-2 and potentially disease severity. *Lancet Infect Dis* 21: e296–e301
- Talic S, Shah S, Wild H, Gasevic D, Maharaj A, Ademi Z, Li X, Xu W, Mesa-Eguiagaray I, Rostron J et al (2021) Effectiveness of public health measures in reducing the incidence of covid-19, SARS-CoV-2 transmission, and covid-19 mortality: systematic review and meta-analysis. *BMJ* 375: e068302
- Thompson KA, Bennett AM (2017) Persistence of influenza on surfaces. *J Hosp Infect* 95: 194–199
- Van Damme W, Dahake R, van de Pas R, Vanham G, Assefa Y (2021) COVID-19: Does the infectious inoculum dose–response relationship contribute to understanding heterogeneity in disease severity and transmission dynamics? *Med Hypotheses* 146: 110431
- van Doremalen N, Bushmaker T, Morris DH, Holbrook MG, Gamble A, Williamson BN, Tamin A, Harcourt JL, Thornburg NJ, Gerber SI et al (2020) Aerosol and Surface Stability of SARS-CoV-2 as Compared with SARS-CoV-1. *N Engl J Med* 382: 1564–1567
- Watson JM, Francis JN, Mesens S, Faiman GA, Makin J, Patriarca P, Treanor JJ, Georges B, Bunce CJ (2015) Characterisation of a wild-type influenza (A/H1N1) virus strain as an experimental challenge agent in humans. *Virology* 12: 13
- Werley MS, McDonald P, Lilly P, Kirkpatrick D, Wallery J, Byron P, Venitz J (2011) Non-clinical safety and pharmacokinetic evaluations of propylene glycol aerosol in Sprague–Dawley rats and Beagle dogs. *Toxicology* 287: 76–90
- World Health Organization (2009) WHO guidelines on hand hygiene in health care
- World Health Organization (2022a) WHO coronavirus (COVID-19) dashboard
- World Health Organization (2022b) Global influenza programme - burden of disease. World Organisation for Animal Health Avian Influenza
- Xiao S, Yuan Z, Yi H (2022) Disinfectants against SARS-CoV-2: a review. *Viruses* 14: 1721
- Zhou J, Peacock TP, Brown JC, Goldhill DH, Elrefaey AME, Penrice-Randal R, Cowton VM, De Lorenzo G, Furnon W, Harvey WT et al (2022) Mutations that adapt SARS-CoV-2 to mink or ferret do not increase fitness in the human airway. *Cell Rep* 38: 110344



License: This is an open access article under the terms of the [Creative Commons Attribution](https://creativecommons.org/licenses/by/4.0/) License, which permits use, distribution and reproduction in any medium, provided the original work is properly cited.